ADVANCED OPTICAL MATERIALS

Supporting Information

for *Advanced Optical Materials,* DOI: 10.1002/adom.201801236

Ultra-Narrowband Metamaterial Absorbers for High Spectral Resolution Infrared Spectroscopy

*Sungho Kang, Zhenyun Qian, Vageeswar Rajaram, Sila Deniz Calisgan, Andrea Alù, and Matteo Rinaldi**

Supporting Information

Design of Ultra-Narrowband Spectral Resolution Metamaterial Absorbers for High Spectral Resolution Infrared Spectroscopy

*Sungho Kang, Zhenyun Qian, Vageeswar Rajaram, Sila Deniz Calisgan, Andrea Alù, and Matteo Rinaldi**

1. Numerical simulation

The finite integration technique, using the commercial software Computer Simulation Technology (CST) Microwave Studio, was utilized to validate angular insensitivity as well as to study field distributions of the narrowband MIM IR absorbers. A unit cell with periodic boundary settings was first constructed to simulate an array of the cross-shaped nanostructures. The Drude model material parameters for gold are obtained from Rakić, A. D. *et al.* and used for the cross-shaped nanostructures and the continuous ground plane.[44] The fitting parameters for Brendel oscillator to model optical properties of silicon dioxide were obtained from Kischkat, J. *et al.*[38] For simulating angular insensitivity, the angle of incidence was swept from 0° to 70° with both TE and TM polarizations (η_{TE} and η_{TM}). The absorptance of unpolarized waves ($\eta_{unpolarized}$) was then calculated as $\eta_{unpolarized} \approx (\eta_{TE} + \eta_{TM})/2$. As shown in **Figure S1**, the cross-shaped nanostructure exhibits electric dipole resonance along the direction of incident electric field (parallel to the *x*-axis) while the magnetic resonance (parallel to the *y*-axis) due to the anti-parallel currents can be seen in the cross section.

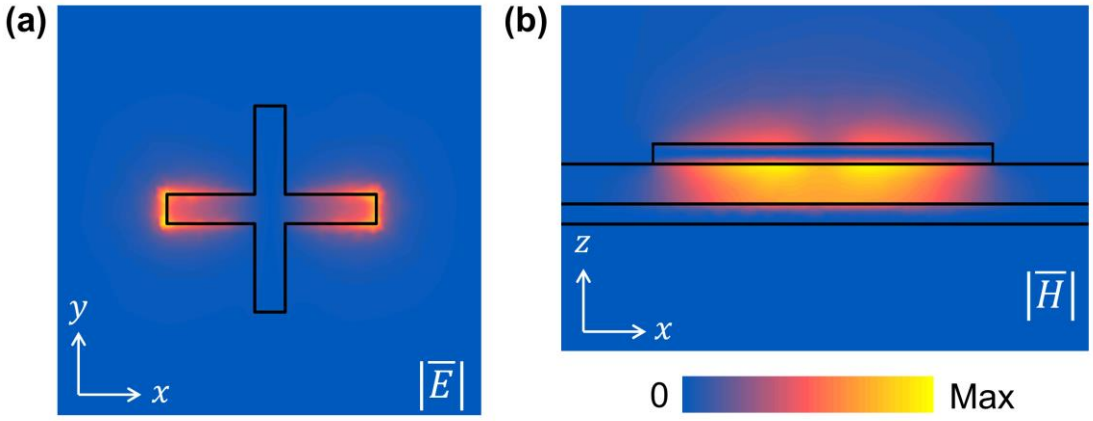

(S1)

Figure S1. **Simulated color maps of narrowband MIM IR absorbers.** The electric and magnetic fields of the incident waves are polarized along the *x*-axis and *y*-axis, respectively. (a) The electric field intensity from the top view and (b) the magnetic field intensity from the cross-sectional view of a unit cell at the peak absorption.

2. Effective lumped elements for oblique incident angles

Although the transmission-line model assumes that the incident electromagnetic waves impinge at normal incidence ($\theta_{TM} = \theta_{TE} = 0^{o}$), angular absorption response can be approximated by using the effective geometric parameters. For an oblique incident angle, we assume only the normal component of the incident waves contributes to the absorption response. Since the normal component of the wave vector ($k_{\perp}$) with an incident angle of θ_i, can be written as $k_{\perp} = kcos\theta_i$, we construct the effective geometric parameters for the gap between neighboring cross-shaped nanostructures ($\Lambda - b$) and the dielectric spacer (t_{ox}) for different polarizations. That is, for transverse magnetic (TM) polarized waves, $\Lambda - b$ in C_P is replaced with $(\Lambda - b)/\cos\theta_{TM}$; whereas for transverse electric (TE) polarized waves, we replace t_{ox} with $t_{ox}/\cos\theta_{TE}$ in L_m and C_m as follows. Note that L_m and C_m for TM polarization (magnetic field is always parallel to the y-axis) and C_p for

TE polarization (electric field is always parallel to x-axis) remain the same as those of normal incidence (Equation 1-3).

$$C_{P,TM} = \pi\varepsilon_0 \frac{a}{ln\left(\frac{2\left(\frac{\Lambda - b}{\cos\theta_{TM}}\right)}{t_{Au}} + \sqrt{\left(\frac{2\left(\frac{\Lambda - b}{\cos\theta_{TM}}\right)}{t_{Au}}\right)^2 - 1}\right)} \quad \text{(S1)}$$

$$L_{m,TE} = \frac{1}{2}\mu_0 \frac{\left(\frac{t_{ox}}{\cos\theta_{TE}}\right) b}{a} \quad \text{(S2)}$$

$$C_{m,TE} = c\varepsilon_0\varepsilon_{ox} \frac{b}{2} \frac{a}{\left(\frac{t_{ox}}{\cos\theta_{TE}}\right)} \quad \text{(S3)}$$

3. Derivation of kinetic inductance (L_k) and resistance (R)

Represented as an inductor in lumped circuit analogy, kinetic inductance expressed in Equation 4 and 6 models the phase delay in high frequency current flow, induced by the finite inertia of charging carriers in a conductive material (Au). This phenomenon is effectively described in the Drude conductivity model (Equation S1) as a function of DC conductivity (σ_{DC}), angular frequency (ω), and relaxation time (τ).

$$\sigma(\omega) = \frac{\sigma_{DC}}{1 + j\omega\tau} \quad \text{(S4)}$$

In the Drude model, conductivity of a metal at high frequency regime is described as frequency dependent complex values, in which the real and imaginary parts contribute to the resistive and inductive components, respectively. That is, the impedance of the gold cross-type nanostructures

is divided into two parts (real and imaginary parts) to form R_c and $L_{k,c}$ as lumped circuit elements as shown below.

$$Z_c = \frac{b'}{a\delta_{Au}}\frac{1}{\sigma_{Au}(\omega)} = \frac{b'}{a\delta_{Au}}\left(\frac{1+j\omega\tau_{Au}}{\omega_p^2\varepsilon_0\tau_{Au}}\right) = R_c + j\omega L_{k,c} \quad \text{(S5)}$$

The kinetic inductance of a conductive material can be derived in an alternative way, by equating its kinetic energy ($E_{kinetic} = \frac{1}{2}Mv^2$) and magnetic energy ($E_{magnetic} = \frac{1}{2}L_kI^2$). Here, M is the total mass of the charges and v is their velocity. The kinetic energy of gold cross-type nanostructures, therefore, can be expressed explicitly in terms of the geometric dimensions (a, b, δ_{Au}), electron mass (m_e), density (n), and charge (e) (Equation S3). Note that ω_p denotes the plasma frequency of gold and is written as $\omega_p = \sqrt{\frac{ne^2}{m_e\varepsilon_0}}$. Following the methods discussed above, one can express $L_{k,c}$ of the cross-type absorbers as shown in Equation S5.

$$E_{kinetic} = \frac{1}{2}Mv^2 = \frac{1}{2}(m_e na\delta_{Au}b')\left(\frac{I}{a\delta_{Au}bne}\right)^2 = \frac{1}{2}\left(\frac{b'}{a\delta_{Au}}\frac{1}{\omega_p^2\varepsilon_0}\right)I^2 \quad \text{(S6)}$$

$$E_{magnetic} = \frac{1}{2}L_{k,c}I^2 \quad \text{(S7)}$$

$$L_{k,c} = \frac{b'}{a\delta_{Au}}\frac{1}{\omega_p^2\varepsilon_0} \quad \text{(S8)}$$

Note that b' is the effective length of the cross nanostructures ($b' = c' \times b$), which is smaller than the designed length due to the uneven current distribution as shown in **Figure S2**a. The correction factor c' is approximated to be $c' = 1–c$, which is related to the non-uniform electric field

distribution (Figure S2b). R_g and $L_{k,g}$ for the continuous ground plane can be derived in the same manner. However, the current distribution in the ground plane is different than that of the cross-shaped nanostructure, so we approximate the effective width (a') to be approximately half the length (a' = 0.5×b) of a cross-shaped nanostructure for calculations of R_g and $L_{k,g}$.

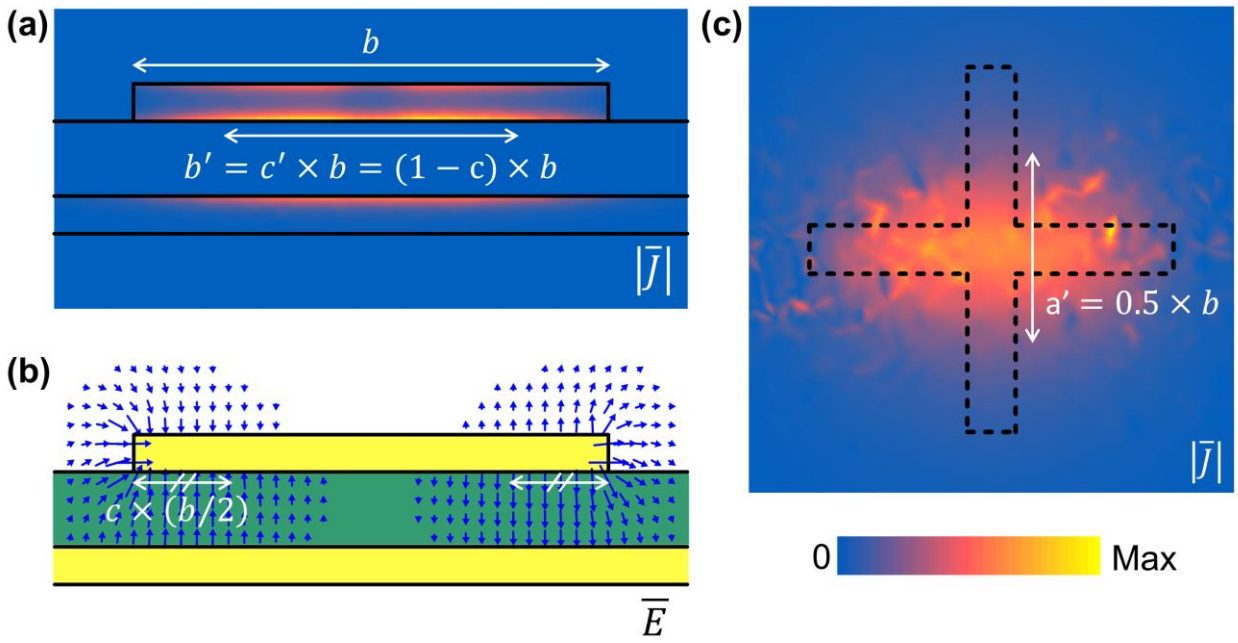

Figure S2. The effective geometric dimensions for the narrowband MIM IR absorbers. (a) The color map of the current density and (b) electric field distribution from cross-sectional view. (c) The color map of the current density in the continuous ground plane. The top nanostructure is outlined as dashed lines for reference. The double arrows indicate the effective dimensions used for lumped circuit elements.

4. Estimation of f_{peak} as a function of circuit parameters

When designing the narrowband infrared absorbers for spectroscopy applications, the capability to tune the peak frequency is an important property. In this section, we take advantage of the modified

circuit model to estimate the peak absorption frequency (f_{peak}) in terms of the circuit parameters. Note that the total impedance, $Z_{cross} = R_{cross}(\omega) + jX_{cross}(\omega)$, is a complex number ($R_{cross}(\omega)$ and $X_{cross}(\omega)$ are the real and imaginary parts of Z_{cross}, respectively) and therefore solutions do not necessarily exist when solving for $Z_{cross}(\omega) = Z_0 \approx 377 + j0\ \Omega$. Instead, we equate the imaginary part of the total impedance to zero, i.e. $X_{cross} = 0$, to estimate the resonant frequency. The total impedance of the cross-type absorbers can be written as below in Laplace domain ($s = j\omega$), where Z_e and Z_m are the impedance of electric and magnetic dipole branches, respectively (Equation S6-S8). Note that inductances for the gold nanostructures ($L_c = L_{k,c} + L_m$) and the continuous ground ($L_g = L_{k,g} + L_m$) plane are combined in the equations for simplicity. The real and imaginary parts of impedance of the cross-type absorber, shown in Figure 3c and Figure 3d of main text, are plotted in **Figure S3**.

$$Z_{cross}(s) = Z_e + Z_m \tag{S9}$$

Where

$$Z_e(s) = \frac{1}{sC_P} \tag{S10}$$

$$Z_m(s) = \frac{s^3 C_m L_c L_g + s^2 C_m\left(L_c R_g + L_g R_c\right) + s\left(C_m R_c R_g + 2L_c\right) + 2R_c}{2 + s^2 C_m\left(L_c + L_g\right) + sC_m(R_c + R_g)} \tag{S11}$$

To estimate the peak frequency, one can solve for $s_{peak} = j\omega_{peak} = j2\pi f_{peak}$ at which the imaginary part of $Z_{cross}(\omega)$ equal to zero. The estimated peak frequency can be expressed in terms of circuit parameters as below (Equation S9).

$$f_{\text{peak}} = \frac{1}{2\pi}\sqrt{\frac{1}{\mathrm{C_m}(L_c + L_g)}} \cong \frac{1}{2\pi}\sqrt{\frac{1}{\mathrm{C_m}(L_k + L_m)}} \quad \text{(S12)}$$

The corresponding absorption spectrum is calculated using transmission line theory ($A = 1 - R_{in} = 1 - |\Gamma_{in}|^2 = 1 - |\, Z_{cross} - Z_0/Z_{cross} + Z_0\,|^2$) and shown in Figure S3 for comparison.

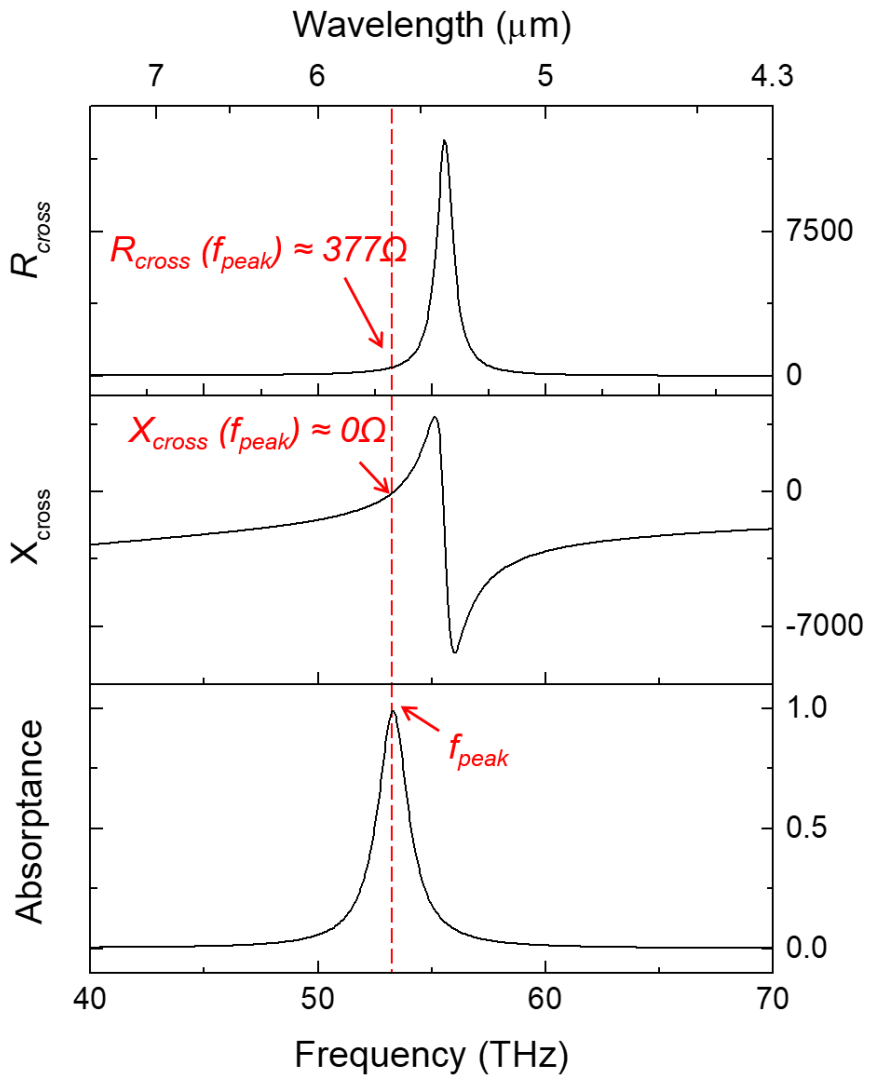

Figure S3. The real (R_{cross}) and imaginary (X_{cross}) parts of the circuit impedance (Z_{cross}) and the absorptance of the cross-type metamaterial infrared absorber shown in Figure 2b of main text.

The peak absorption frequency of the absorber is approximately equal to the resonance of the RLC equivalent circuit, i.e. $X_{cross}|_{f=f_{peak}} \approx 0\Omega$ and $R_{cross}|_{f=f_{peak}} \approx 377\Omega$.

5. Device fabrication

The 12 ultranarrow bandwidth MIM absorbers are fabricated on a p-type silicon wafer. Each MIM IR absorber consists of an array of cross-type nanostructures in 150×150 μm^2 fabricated on the same substrate, with the lateral dimensions (*a*, *b*, and *Γ*) as the only variables (Table S1). The geometric parameters of each absorber are optimized to exhibit narrowband (*FWHM* ≈ *3%*) absorption. We start with electron-beam evaporation of titanium-gold-titanium (10-100-10 nm) to form the ground layer (**Figure S4**a). The first titanium (Ti) layer is to promote adhesion between the Si substrate and the gold (Au) ground layer, whereas the second Ti layer is for the adhesion between the ground layer and the subsequent deposition of dielectric spacer. The thin dielectric spacing is formed by deposition of silicon dioxide (SiO_2) using a PECVD (Plasma Enhanced Chemical Vapor Deposition) system (Figure S4b). Lift-off-resist (LOR) and PMMA were spin-coated and electron beam lithography was performed to expose PMMA and pattern the cross-type nanostructures. It is worth noting that the two-material stack (LOR and PMMA) for patterning the nanostructures is adopted to prevent sidewall residues during the lift-off process, which may deteriorate the absorption selectivity. Furthermore, in order to precisely control the undercut of the cross-type nanostructures, LOR is baked at a higher temperature (200 °C) and the diluted TMAH-based developer is used to develop LOR at a slower speed. After exposing, PMMA is developed using a MIBK:IPA solution, followed by LOR development to form the desired undercuts. The reduced etch rate of LOR (~1nm per second) enables a precise control of the undercuts (Figure S4f) for the periodic nanostructures. Finally, a 10-100 nm Ti-Au layer is deposited via electron

beam evaporation and LOR-PMMA stack was removed by soaking the sample in photoresist remover at an elevated temperature.

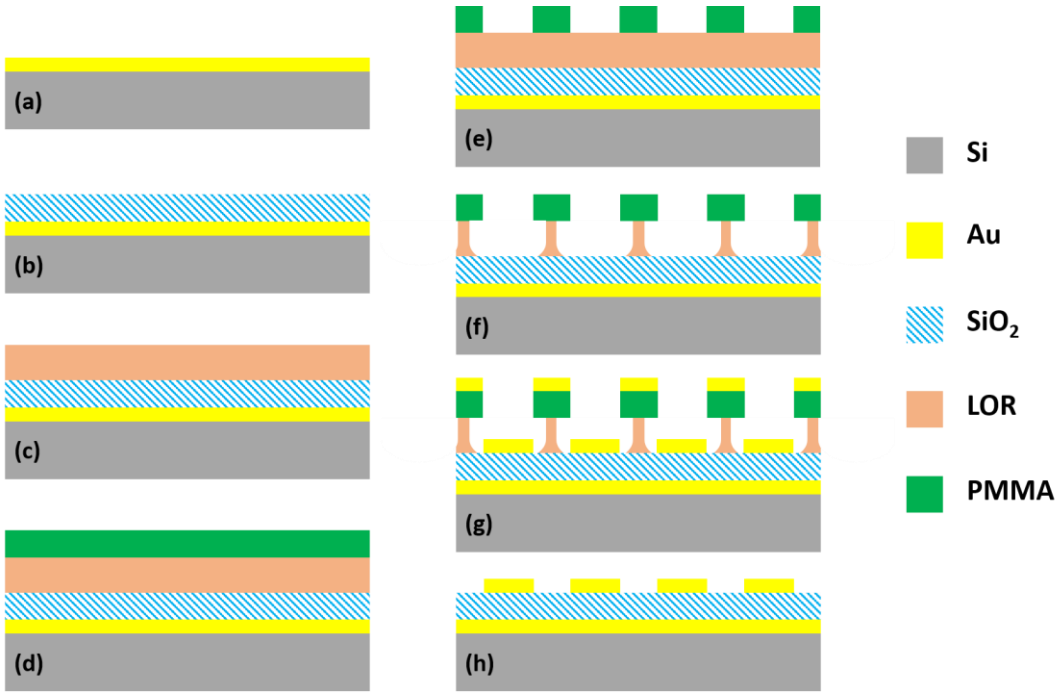

Figure S4. Cross-section schematics of the device fabrication process. (a) 100 nm gold is evaporated on a silicon substrate. (b) 200 nm silicon dioxide is deposited using plasma-enhanced chemical vapor deposition systems. (c) Lift-off-resist (LOR) is spin-coated and baked at 200°C for 5 minutes. (d) PMMA is spin-coated then exposed using an electron beam writing system. (e) PMMA is first developed using MIBK:IPA (1:3) solution for 60 seconds; (f) then LOR is etched to create the desired undercut using diluted TMAH-based developer. (g) 100 nm gold is evaporated. (h) Lift-off of LOR-PMMA stack to pattern the cross-type nanostructures.

Table S1. Optimized lateral dimensions (*a*, *b*, and *Λ*) of the 12 MIM IR absorbers for high spectral selectivity and absorptance

Sample Number	Measured λ_{peak} [μm]	Width (*a*) [nm]	Length (*b*) [μm]	Periodicity (Λ) [μm]
Absorber 1	4.27	150	1.3	3.0
Absorber 2	4.54	150	1.4	3.2
Absorber 3	4.89	200	1.5	3.4
Absorber 4	5.11	200	1.6	3.6
Absorber 5	5.36	200	1.7	3.6
Absorber 6	5.58	200	1.8	3.8
Absorber 7	5.83	200	1.9	4.0
Absorber 8	6.05	300	2.0	4.0
Absorber 9	6.27	300	2.1	4.0
Absorber 10	6.48	300	2.2	4.0
Absorber 11	6.63	300	2.3	4.0
Absorber 12	6.78	300	2.4	4.0